CFD-driven optimization of a Venturi tube for wastewater treatment applications

Francesco De Vanna[a], Alberto Benato[b (CA)], Matteo Ballan[c] and Anna Stoppato[d]

[a] Department of Industrial Engineering - University of Padova, Padova, Italy, francesco.devanna@unipd.it
[b] Department of Industrial Engineering - University of Padova, Padova, Italy, alberto.benato@unipd.it (CA)
[c] Department of Industrial Engineering - University of Padova, Padova, Italy, matteo.ballan@studenti.unipd.it
[d] Department of Industrial Engineering - University of Padova, Padova, Italy, anna.stoppato@unipd.it

Abstract:

The paper presents a procedure for a systematic numerical optimisation of a Venturi tube for water treatment using cavitation conditions. The numerical method employs computational fluid dynamics techniques within a Reynolds-Averaged Navier-Stokes framework in conjunction with an optimisation procedure to improve a baseline Venturi configuration. To define the numerical model associated with the baseline solution, a reliable meshing method is given. The procedure evaluates various mesh sizes and turbulence closure to determine the ideal balance between processing time and accuracy. The model is then used as a starting point for an optimisation procedure. The optimised arrangement improves the mean vapour quality of the tube by approximately 130% compared to the original geometry.

Keywords:

Hydrodynamic cavitation; Venturi tube; CFD investigation; wastewater treatment.

1. Introduction

Hydrodynamic cavitation is a well-known phenomenon gaining prominence due to its use in various technical and chemical processes, such as emulsification, oxidation, nanomaterial production, and wastewater treatment. Hydrodynamic cavitation aims to induce cavitating microbubbles into the water flow, and the Venturi tube is a commonly adopted device for this purpose.

The Venturi tube is a simple device that consists of a converging section where the flow is accelerated, a throat zone where the pressure reaches its lowest value, and a diverging segment where the tube recovers the cross section of the pipe in which it is placed. If the ratio between the Venturi throat diameter and the diameter of the external pipe is small enough, the increase in velocity induced by section reduction can lead to cavitating conditions in the throat flow. When the static pressure falls below the vapour pressure, cavitation is defined as the development, growth, and collapse of microbubbles or vapour cavities in a liquid. Due to the adiabatic compression of the cavities, the collapse occurs at various points. Consequently, a substantial amount of energy is quickly released, generating a supercritical state with high temperature and pressure (5000 K and 500 bar) similar to those on the solar surface. These conditions accelerate chemical and physical transformations, which can be used for a variety of practical applications, including the destruction of chemical contaminants in water (Gogate et al. [1], Dular et al. [2], Sarc et al. [3], Biasiolo et al. [4]).

Carpenter et al. [5] sum up the theory of cavitation, focussing on the hotspots of collapsing cavities, and discuss the available approaches to generate the multiphase phenomena and the corresponding uses of the technology in different contexts. Researchers emphasised the importance of the specific geometric characteristics of the Venturi tube.

Using Computational Fluid Dynamics (CFD) techniques, Dastane et al. [6] numerically analysed the cavitating flow in a Venturi tube, comparing various mesh sizes and performing single- and multiphase simulations. They observed that the single-phase method underestimates the value of the input pressure. Bashir et al. [7] offer a CFD-based optimisation technique for the geometry of cavitating Venturi tubes. Using experimental tests and simulations, Li et al. [8] explored the impact of Venturi geometries on cavitation.

Despite the already published work, the prediction of cavitating flows using computational methods is still a critical issue, and only few results are available in the literature. In particular, the most advanced CFD strategies, such as Large-Eddy Simulations (LES) and Direct Numerical Simulations (DNS), can hardly be adopted in multiphase and complex flow conditions, such as those about a deep cavitating wall-bounded flow. Therefore, digital prototyping of such devices is still demanded by Reynolds-Averaged Navier-Stokes (RANS) based models, albeit with all the limitations that such strategy embeds.

https://doi.org/10.52202/069564-0045

The present work aims to determine the most critical parameters that influence the RANS CFD simulation results for flow cavitation inside Venturi tubes and to provide optimisation suggestions to enhance the Venturi baseline design. A RANS model has been built and used to predict the two-phase flow and to make a comparison between various model resolutions in terms of grid discretization level. The results indicate that high grid resolutions are required for numerically insensitive outcomes. Finally, the baseline model is used as a starting point for an optimisation procedure devoted to design a novel tube shape capable of improving steam generation.

The paper is organised as follows: Section 2. presents the numerical model and provides a description of the numerical settings. Section 3. summarises and discusses mesh sensitivity analysis with the aim of finding the optimal mesh size. Section 4. provides hints regarding the Latin Hypercube Sampling (LHS) method implemented to optimise the Venturi geometry and gives quantitative information concerning the characteristics of the tube shape. Finally, Section 5. gives the concluding remarks.

2. Computational setup

The development of a Venturi tube optimised configuration requires the development of a properly calibrated numerical model of the device. To this end, the University of Padova research group (Turbomachinery and Energy Systems - TES Group), after an in-depth review of the literature, has selected the baseline geometry of the Venturi tube (see De Vanna et al. [9]). The developed model reproduces the geometry proposed by Shi et al. [10]. The baseline geometry is used to (i) correctly set the numerical model, (ii) determine the most appropriate grid dimension, and (iii) choose the reliable turbulence model.

Figure 1 shows the shape of the baseline configuration, while Table 1 lists the dimensions of the Venturi tube. The device has a throat diameter (d) of 3.18 mm, while the diameter of the pipe (D) is equal to 12.7 mm. The converging angle slopes is of 19° while the diverging one is equal to 5°. The CFD model is extended by 30 and 80 mm before and after the L_1 and L_5 segments to achieve fully developed turbulent flow and prevent unphysical recirculations. The axial symmetry of the tube limits the task to a 2D domain. Ansys-Workbench 2020 R1 is used to build both geometry and grids, while Ansys-Fluent is used to solve the flow field [11].

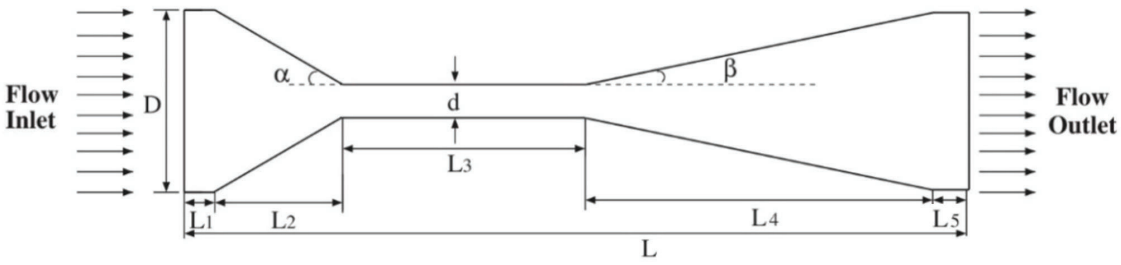

Figure 1: Schematic view of the Venturi tube geometry. Dimensions are listed in Table 1.

Table 1: Geometry characteristics of the baseline shape of the Venturi tube as given by Shi et al. [10].

D (mm)	d(mm)	L_1 (mm)	L_2 (mm)	L_3 (mm)	L_4(mm)	L_5 (mm)	α (°)	β (°)
12.7	3.18	6.00	14.0	20.0	54.0	6.00	19.0	5.00

Based on the experience of the research team in the field of CFD, three structured meshes of 100′000 (100k), 200′000 (200k) and 300′000 (300k) elements have been built and tested with the aim of finding the dimension of the grid that guarantees a good compromise between the accuracy of the results and the efficiency of the computation.

Adopting the internal software suites, each computational grid is quality validated to ensure a maximum skewness value below 0.22, an inflation growth rate between 1.05 and 1.20, and an orthogonality quality value above 0.99. Inflation is placed close to the walls to improve the resolution in the boundary layer and ensure that the wall Y plus (defined as $y^+ = y_w/\delta_\nu$, $\delta_\nu = \mu_w/(\rho_w u_\tau)$) values are accurate. δ_ν is the wall viscous length while ρ_w and μ_w are the fluid density and viscosity at the location of the wall, respectively. u_τ is the friction velocity, while y_w is the first-off-the-wall cell distance. Specifically, the objective is to address a y^+ value lower than 1. Table 2 reports the mean aspect ratio, the mean skewness and the mean orthogonal quality of the three developed meshes while Figure 2 shows an extent zoom of the 300k grid in the Venturi inflowing corner.

https://doi.org/10.52202/069564-0045

Table 2: Grid quality parameters.

Mesh	Mean aspect ratio	Mean Skewness	Mean Orthogonal quality
100k	4.194	$2.80 \cdot 10^{-2}$	0.996
200k	4.508	$2.73 \cdot 10^{-2}$	0.996
300k	6.091	$2.21 \cdot 10^{-2}$	0.997

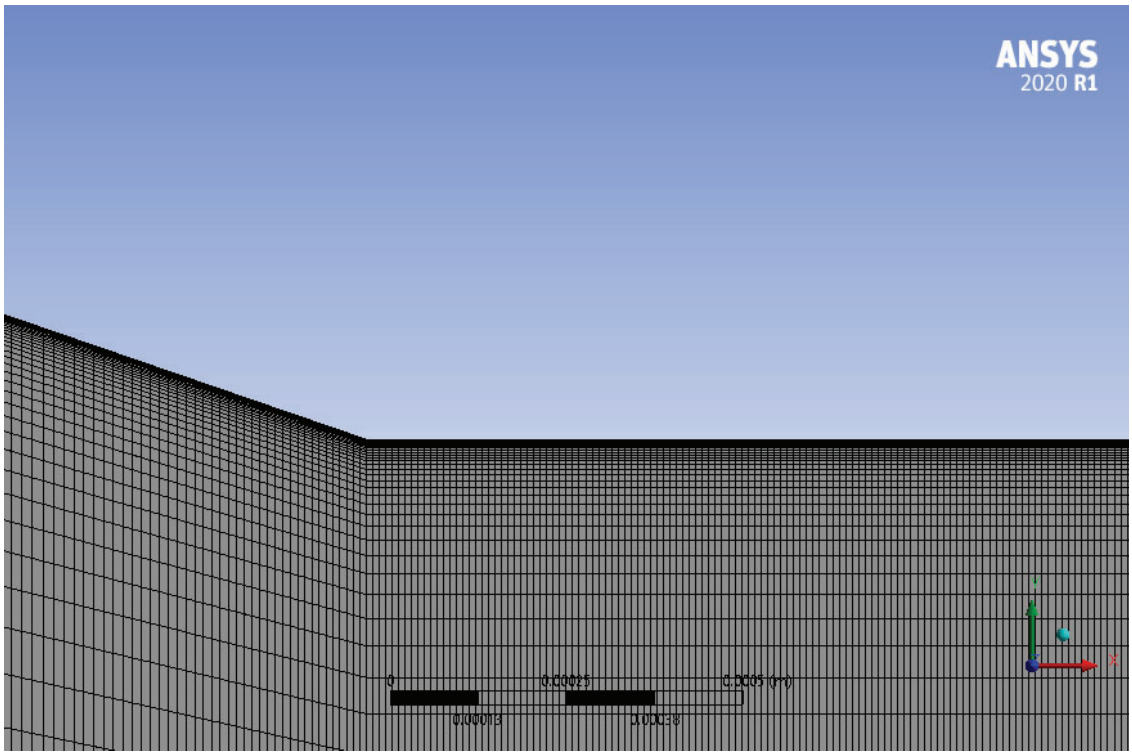

Figure 2: Detailed view of the 300k mesh in the inflowing Venturi corner.

The system's dynamics is simulated by finding solutions to an incompressible RANS system of equations in a steady-state framework. The flow field dynamics is solved using four different turbulence models. As said, the test of different turbolence models is used to find the best compromise between accuracy and calculation time.

The complexity of the model gradually increases from first to last: the one-equation Spalart-Allmaras (SA) model, the two-equations k-epsilon realisable model, the two-equations k-omega shear stress transport (SST) model, and the four-equation transition SST (TSST) model.

To solve the mass and momentum conservation equations related to the behaviour of the cavitating flow in the mixture model, the pressure-velocity coupled method is adopted. Thus, to satisfy the requirements of the coupling algorithms, the equations include implicit discretization of the pressure gradient terms and the mass flow.

To discretise the convective components in the transport equations for the vapour volume fraction, the Quadratic Upwind Interpolation for Convection Kinematics (QUICK) technique is used. The PREssure STaggering Option (PRESTO) method is adopted in the computation of the pressure. To discretize the convection terms that are included in the momentum equations, the second-order upwind technique is selected. Finally, the "water-vapor" mixture model is adopted to mimic two-phase cavitation flows for multiphase flow solutions. The phase transition is computed according to the Schnerr-Sauer cavitation model. As boundary conditions, the "pressure inlet" and "pressure outlet" conditions are enforced at the inflowing and outflowing edges, respectively; this means setting the total and static pressure. Additionally, "adiabatic no-slip wall" conditions are enforced at the Venturi internal surfaces. In the nameplate conditions, a condition that embeds cavitating events in the throat of the tube is set. This means an inlet total pressure, p°_{in}, of 180'000 Pa and a static pressure at the

outlet, p_{out}, of 101'325 Pa.

3. Baseline Venturi model validation procedure

The validation process of the developed model aims to define the most suitable turbolence model and grid size. First, mesh sensitivity analysis is performed with the total intake pressure set at its design value (180 kPa). The process follows CFD best practises according to De Vanna et al. [12]. Figure 3 provides the freestream-scaled axial velocity, u/u_∞, and pressure, p/p_∞, distributions along the throat-scaled axial coordinate, $x^* = x/d$, as a function of both the grid resolution and the turbulence model. As shown in Figure 3, results are clustered in a really narrow band, except for the results obtained with the SA model and in the coarser cases. Therefore, the comparison allows to certainly exclude the simplest turbulence model as well as the mesh with the lower resolution.

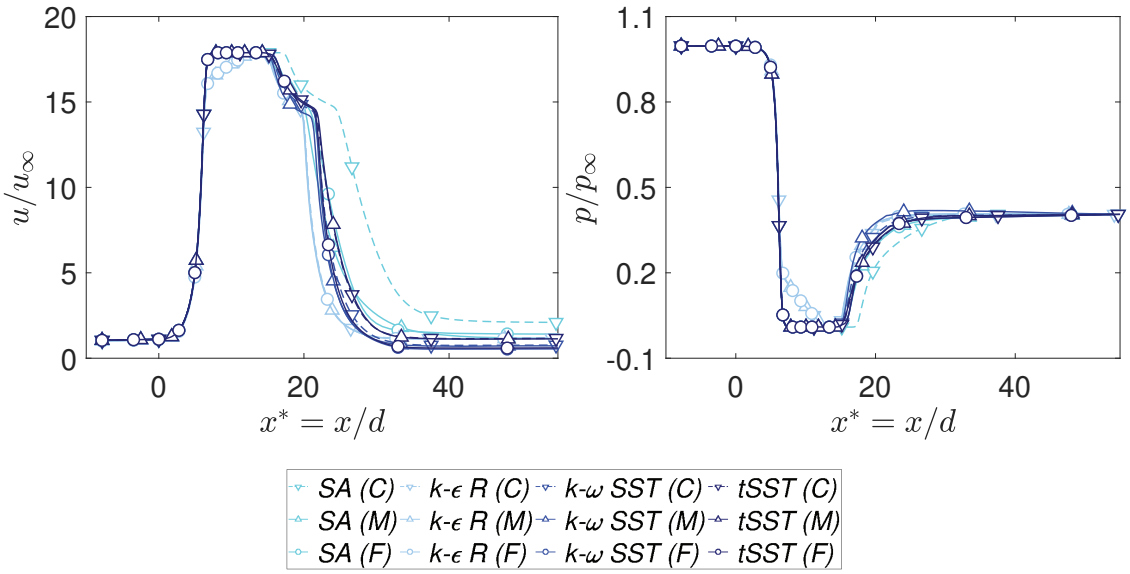

Figure 3: Axial velocity and pressure distributions as a function of the grid refinement and turbulence model. The lighter to darker tone of the colour refers to gradually more complex turbulence models, i.e. SA, $k-\epsilon$ realisable, $k-\omega$ SST and TSST, respectively.

The global parameters are compared to fine-tune the grid and assess the influence of the discretization level on the investigation results. Figure 4 depicts the non-dimensional Venturi pressure drop and the coarse-scaled drag force as a function of the grid resolution. The 100k element mesh somewhat underestimates the drop in pressure, but the model saturates the value after 200k grid refinements. Instead, the drag coefficient data are exactly matched as the grid size changes. This implies that an excessive number of mesh elements would be unreasonable, which would only result in stressing computer resources. Based on the evaluation of global parameters, the 200k configuration seems to be the ideal trade-off between numerical accuracy and computing load. Thus, the 200k mesh arrangement, combined with the k-omega SST, is selected and used for the upcoming analyses.

4. Latin Hypercube Sampling and optimisation results

In this work, the Latin Hypercube Sampling (LHS) technique is used to improve the design of the Venturi geometry regarding a priori specified goals. The LHS technique has been proposed by McKay et al. [13] as a sampling mechanism to fill a design variable space. The importance of sampling is derived from the need to correctly choose the input variables of a mathematical model that describes real occurrences, thus gathering the necessary information about the probability distribution of the output with the fewest number of inputs. Swiler et al. [14] define Latin Hypercube Sampling as a technique to examine the probability distribution of a multivariate function with k variables by selecting n different values for each variable. Using the equal probability reasoning, the values are selected by dividing each variable into n different pieces. As a result, after randomly selecting a value from each layer, the values collected for each variable are randomly paired, producing n evaluations of the input variables. Loh [15] provided a more detailed examination of the theoretical

https://doi.org/10.52202/069564-0045

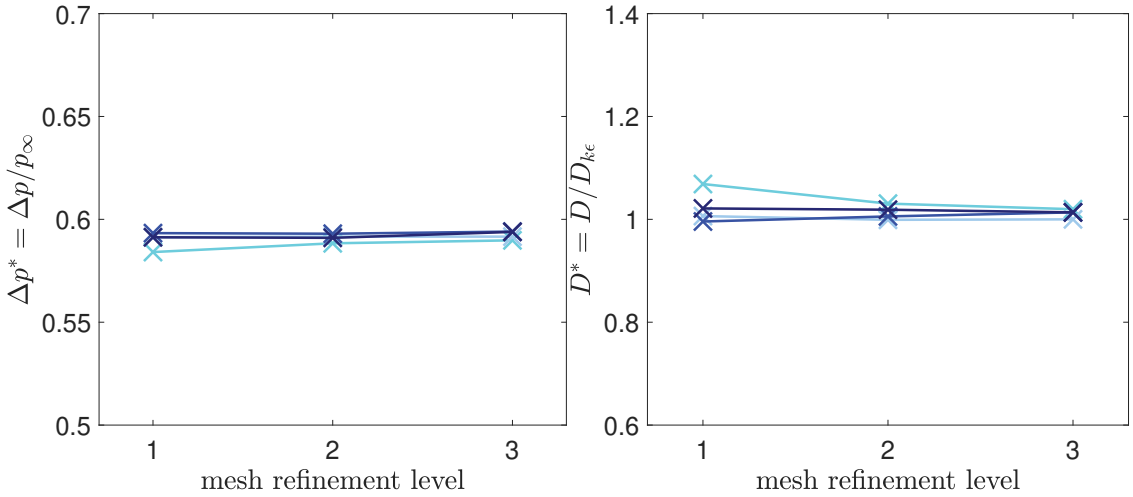

Figure 4: Model validation as a function of the grid refinement and turbulence model. From lighter to darker tones colours refer to gradually more complex turbulence models, i.e., SA, $k-\epsilon$ realisable, $k-\omega$ SST and TSST, respectively. The refinement level refers to the 100k, 200k, and 300k mesh, respectively.

background of the LHS approach, as well as the fundamental mathematical formulation of the method. As presented by Helton et al. [16], this technique has been widely used in complex system analyses, with its main characteristics highlighted, such as its simplicity and ability to result in more uniform stratification than other random sampling strategies, revealing to be a suitable method for selecting input variables or having a rough estimate of optimal locations. In this study, the Latin Hypercube Sampling technique is employed using the Matlab "lhsdesign" function, which generates an LHS matrix of size $k \times n$, where k and n are again variables and different values for each variable, respectively. In particular, each configuration generated by the LHS method consists of a variation of the baseline solution reconstructed through Beziér splines. The approach allows to obtain different Venturi tube geometries in terms of shape angles, inlet, throat, and discharge lengths, as well as it ensures a smooth profile of the tube.

To assess the performance of the geometric configurations of the Venturi tube in terms of the ability to generate cavitation events, each configuration has been assigned a performance parameter related to the generation of steam in the discharge portion of the pipe. Five stations (named *stat*1, *stat*2, *stat*3, *stat*4, *stat*5) are placed beside the tube discharging section to sample the radial distribution of the vapour quality. The average integral value of the steam quality, X_v, is derived for each distribution according to Equation 1:

$$X_v(x_i) = \frac{1}{R}\int_0^R X_v(x_i, r)dr, \quad i = 1, \dots, N_{stats} \tag{1}$$

where r and R denote the radial coordinate and the maximum radius associated with each station, respectively, while x_i are the axial coordinates of the samples. As a result, this value indicates how much steam is connected to each station. Finally, the five measurements associated with each station are averaged to provide a single performance parameter for each geometric arrangement, i.e.,

$$X_v = \frac{1}{N_{stats}}\sum_{i=1}^{N_{stats}} X_v(x_i) \tag{2}$$

When applied to the baseline Venturi's configuration, this method produces a performance metric of X_v = 0.1421. Instead, the LHS optimisation process produces a set of 12 configurations capable of greatly enhancing the performance inherent in steam generation compared to the baseline (see Table 3).

Table 3: Results of the optimisation analysis.

Configuration	Vapor performance index	Improvement [%]
baseline	0.1421	-
1	0.2688	89.11
2	0.2382	67.59
3	0.2825	98.75
4	0.1734	22.01
5	0.1933	36.02
6	**0.3321**	**133.7**
7	0.2138	50.40
8	0.1627	14.48
9	0.1455	2.38
10	0.2275	60.05
11	0.1931	35.88
12	0.1451	2.10

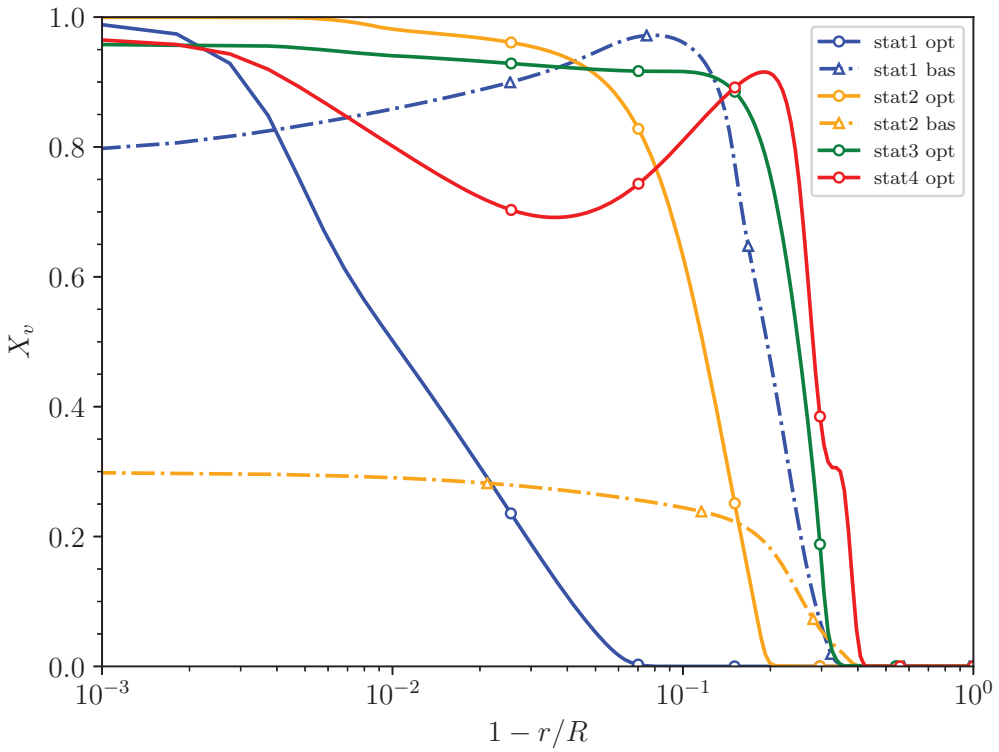

Figure 5: Baseline and optimal solutions comparison in terms of steam production distribution in the Venturi discharging sections.

Although all factors considered result in a significant boost in steam production performance, individual 6 is unquestionably the best. In fact, it is observed a 133% increase in the steam generation on average when compared to the baseline solution. Figure 5 compares the trend in steam quality at the five stations in configuration 6 with the same data acquired in the baseline situation. The solid curves represent the optimal case, while the dashed-dotted curves report the baseline solution. It can also be seen that the baseline configuration tends to cluster the vapour production in the early stations, with the first station having a clear advantage. Furthermore,

https://doi.org/10.52202/069564-0045

stations 1 and 2 of the baseline solution (in Figure 5 (named *stat*1 and *stat*2) concentrate the quality of the vapour along the wall of the pipe. Instead, the optimal solution not only improves the steam distribution in *stat*1 and *stat*2, but also generates a significant amount of steam in *stat*3 and *stat*4 (see Figure 5), whereas the baseline does not. For completeness, it is reasonable to claim that stations with a vapour quality less than 10^{-2} are not meaningful and, therefore, are not reported.

5. Conclusions

The proposed investigation examines a baseline and an improved Venturi tube geometry for applications involving hydrodynamic cavitation. After building the numerical model of the device, it is first calibrated as a function of grid resolution and turbulence model, with a focus on the independence of the results from mesh refinement. The baseline model is then used as the leading configuration in an LHS-based automatic optimisation process. Compared to the baseline configuration, the method can increase the steam production of the Venturi tube by almost 130%. In addition, the improved design concentrates steam production along the channel axis, while the baseline design directs steam production toward the wall. Therefore, the study demonstrates that by modifying the Venturi tube design, the hydrodynamic system performance can be improved. Without chemical components, solvents, and/or addition of man-made substances, the optimised geometry can be an economic solution to abate contaminants in water systems. In future studies, experimental campaigns will be conducted in both baseline and optimised configurations to validate numerical findings and/or design new, more efficient Venturi tube configurations. In addition to optimisation and numerical simulations, alternative configurations, including numerous Venturi tubes or asymmetrical nozzles, will be designed and tested.

Acknowledgments

The authors acknowledge Veritas S.p.A. and, particularly, Dr. Graziano Tassinato and Francesco Nisato for the fruitful discussions on Venturi systems for water treatment.

Abbreviations

CFD Computational Fluid Dynamics

DNS Direct Numerical Simulations

LES Large-Eddy Simulations

PRESTO PREssure STaggering Option

QUICK Quadratic Upwind Interpolation for Convection Kinematics

RANS Reynolds-Averaged Navier-Stokes

SA Spalart-Allmarass

SST Shear Stress Transport

TSST Transition Shear Stress Transport

Symbols

α Venturi converging angle, [°]

β Venturi diverging angle, [°]

d Venturi throat diameter, [m]

D Venturi pipe diameter, [m] / Drag force, [N]

δ_ν Viscous length, [m]

Δp Pressure drop, [Pa]

μ_w Wall viscosity, [Pa s]

p_{in}° Inflowing total pressure, [Pa]

p_{out} Outflowing static pressure, [Pa]

ρ_w Wall density, [$kg \cdot m^{-3}$]

u Axial mean velocity, $[m \cdot s^{-1}]$

u_∞ Freestream velocity, $[m \cdot s^{-1}]$

p_∞ Freestream pressure, $[Pa]$

u_τ Friction velocity, $[m \cdot s^{-1}]$

x^* Throat scaled axial coordinate

X_v Vapor quality

y^+ Inner scaled wall distance

References

[1] Gogate, P. R., & Kabadi, A. M. A review of applications of cavitation in biochemical engineering/biotechnology. Biochemical Engineering Journal (2009), 44(1), 60-72.

[2] Dular, M., Khlifa, I., Fuzier, S., Adama Maiga, M., & Coutier-Delgosha, O. Scale effect on unsteady cloud cavitation. Experiments in fluids (2012), 53, 1233-1250.

[3] Sarc, A., Kosel, J., Stopar, D., Oder, M., & Dular, M. . Removal of bacteria Legionella pneumophila, Escherichia coli, and Bacillus subtilis by (super) cavitation. Ultrasonics sonochemistry (2018), 42, 228-236.

[4] Biasiolo M., Ballarin M., Tassinato G., Stoppato A. &, Cavinato, C.. Semi-continuous Chlorella Vulgaris Cultivation Using Anaerobic Digestate Liquid Fraction Pre-treated by Ultrasonic Cavitation to Improve Carbon Dioxide Solubilization. Chemical Engineering Transactions (2022), 92, 151-156.

[5] Carpenter J., Badve M., Rajoriya S., George S., Saharan V.K., Pandit A.B. *Hydrodynamic cavitation: an emerging technology for the intensification of various chemical and physical processes in a chemical process industry.* Rev. Chem. Eng. (2017); 33: 433–468.

[6] Dastane G.G.,Thakkar H., Shah R., Perala S., Raut J., Pandit A.B. *Single and multiphase CFD simulations for designing cavitating venturi* Chemical Engineering Research and Design (2019); 149: 1-12.

[7] Bashir, T. A., Soni, A. G., Mahulkar, A. V., & Pandit, A. B. The CFD driven optimisation of a modified venturi for cavitational activity. The Canadian Journal of Chemical Engineering (2011), 89(6), 1366-1375.

[8] Li M., Bussonnière A., Bronson M., Zhenghe X., Liu Q. *Study of venturi tube geometry on the hydrodynamic cavitation for the generation of microbubbles* Miner. Eng. (2019); 132: 268–274.

[9] De Vanna F., Benato A., Scramoncin A. Stoppato A., *CFD modelling of a Venturi tube for wastewater treatment applications*. In: Elmegaard, B., Sciubba , E., Blanco-Marigorta , A. M., Jensen, J. K., Markussen, W. B., Meesenburg, W., Arjomand Kermani, N., Zhu, T., & Kofler, R., editors. ECOS 2022: Proceedings of the 35th International Conference on Efficiency, Cost, Optimization, Simulation, and Environmental Impact of Energy Systems; 2022 July 1-3; COPENHAGEN, DENMARK. Danmarks Tekniske Universitet (DTU).

[10] Shi, H., Li, M., Nikrityuk, P., Liu, Q. *Experimental and numerical study of cavitation flows in venturi tubes: From CFD to an empirical model*. Chemical Engineering Science (2019), 207, 672-687.

[11] Ansys. *FLUENT 12.0 Theory Guide.* Available at: `https://www.afs.enea.it/project/neptunius/docs/fluent/html/ug/node1.htm` [accessed 9.9.2021].

[12] De Vanna, F., Bof, D., & Benini, E. . Multi-objective RANS aerodynamic optimization of a hypersonic intake ramp at Mach 5. Energies (2022), 15(8), 2811.

[13] McKay, M. D., Beckman, R. J., & Conover, W. J. . A comparison of three methods for selecting values of input variables in the analysis of output from a computer code. Technometrics (2000), 42(1), 55-61.

[14] Swiler, L. P., & Wyss, G. D. (2004). A user's guide to Sandia's latin hypercube sampling software: LHS UNIX library/standalone version (No. SAND2004-2439). Sandia National Laboratories (SNL), Albuquerque, NM, and Livermore, CA (United States).

[15] Loh, W. L. On Latin hypercube sampling. The annals of statistics (1996), 24(5), 2058-2080.

[16] Helton, J. C., & Davis, F. J.. Latin hypercube sampling and the propagation of uncertainty in analyses of complex systems. Reliability Engineering & System Safety (2003), 81(1), 23-69.

https://doi.org/10.52202/069564-0045